Biochimica et Biophysica Acta 1847 (2015) 35–45

Contents lists available at ScienceDirect

Biochimica et Biophysica Acta

journal homepage: www.elsevier.com/locate/bbabio

Review

Fourier transform infrared difference and time-resolved infrared detection of the electron and proton transfer dynamics in photosynthetic water oxidation☆,☆☆

Takumi Noguchi *

Division of Material Science, Graduate School of Science, Nagoya University, Furo-cho, Chikusa-ku, Nagoya, 464-8602, Japan

ARTICLE INFO

Article history:
Received 13 May 2014
Received in revised form 25 June 2014
Accepted 26 June 2014
Available online 3 July 2014

Keywords:
FTIR
Time-resolved infrared spectroscopy
Photosynthesis
Water oxidation
Oxygen evolution
Proton transfer

ABSTRACT

Photosynthetic water oxidation, which provides the electrons necessary for CO_2 reduction and releases O_2 and protons, is performed at the Mn_4CaO_5 cluster in photosystem II (PSII). In this review, studies that assessed the mechanism of water oxidation using infrared spectroscopy are summarized focusing on electron and proton transfer dynamics. Structural changes in proteins and water molecules between intermediates known as S_i states ($i = 0$–3) were detected using flash-induced Fourier transform infrared (FTIR) difference spectroscopy. Electron flow in PSII and proton release from substrate water were monitored using the infrared changes in ferricyanide as an exogenous electron acceptor and Mes buffer as a proton acceptor. Time-resolved infrared (TRIR) spectroscopy provided information on the dynamics of proton-coupled electron transfer during the S-state transitions. In particular, a drastic proton movement during the lag phase (~200 μs) before electron transfer in the $S_3 \rightarrow S_0$ transition was detected directly by monitoring the infrared absorption of a polarizable proton in a hydrogen bond network. Furthermore, the proton release pathways in the PSII proteins were analyzed by FTIR difference measurements in combination with site-directed mutagenesis, isotopic substitutions, and quantum chemical calculations. Therefore, infrared spectroscopy is a powerful tool for understanding the molecular mechanism of photosynthetic water oxidation. This article is part of a Special Issue entitled: Vibrational spectroscopies and bioenergetic systems.

1. Introduction

In the oxygenic photosynthesis performed by plants and cyanobacteria, light energy is converted into chemical energy in the form of sugars using only water and CO_2 as the chemical resources. Water serves as the ultimate electron donor for the reduction of CO_2, and is split into O_2 and protons when oxidized. The protons are released into the thylakoid lumen to produce a proton gradient across the thylakoid membranes, which drives ATP synthesis to serve as an energy source for CO_2 fixation. In contrast, O_2 is liberated into the air, creating an oxygenic atmosphere (21% O_2) that is used for respiration. O_2 is also converted into ozone, which protects life from harmful UV radiation. Therefore, oxygenic photosynthesis is a biological process essential for sustaining the global environment and life on earth as a source of both energy and O_2.

Photosynthetic water oxidation is performed in the photosystem II (PSII) protein complexes [1–8]. In PSII, electron transfer starts from the excited singlet state of the reaction center chlorophylls (the coupled excited state of monomeric chlorophyll Chl_{D1} and chlorophyll dimer P680), which ejects an electron to the pheophytin electron acceptor Pheo, and leads to the formation of a $P680^+Pheo^-$ charged pair [9,10] (Fig. 1A). On the electron acceptor side, an electron is transferred from $Pheo^-$ to the primary quinone electron acceptor Q_A and then to the secondary acceptor Q_B [11]. Upon accepting two electrons, Q_B is converted into a plastoquinole molecule by the uptake of two protons, and is then released into the thylakoid membranes. On the electron donor side, $P680^+$ oxidizes the redox-active tyrosine Y_Z (D1-Y161) followed by the water oxidizing center (WOC), which is the catalytic site of water oxidation [1–8]. Therefore, electrons extracted from water are transferred finally to plastoquinol, via light-driven reactions in PSII, which transports electrons to the Cytb_6/f complex in thylakoid membranes.

X-ray crystallographic structures of PSII complexes [12–14] show that the WOC consists of the Mn_4CaO_5 cluster, two Cl^- ions located ~7 Å away from the closest Mn ions, and surrounding amino acid residues including ligands for the Mn and Ca ions [D1-Asp170, D1-Glu189, D1-Asp333, D1-Asp342, D1-Ala344 (C-terminus), CP43-Glu354, and D1-His332] (Fig. 2). A recent high-resolution (1.9 Å) X-ray structure [14] further resolved the water ligands: W1 and W2

☆ This article is part of a Special Issue entitled: Vibrational spectroscopies and bioenergetic systems.
☆☆ This article is dedicated to the memory of Warwick Hillier (Oct. 18, 1967–Jan. 10, 2014), who made significant contributions to the water oxidation researches using FTIR spectroscopy and mass spectrometry.
* Tel.: +81 52 789 2881; fax: +81 52 789 2883.
E-mail address: tnoguchi@bio.phys.nagoya-u.ac.jp.

http://dx.doi.org/10.1016/j.bbabio.2014.06.009
0005-2728/

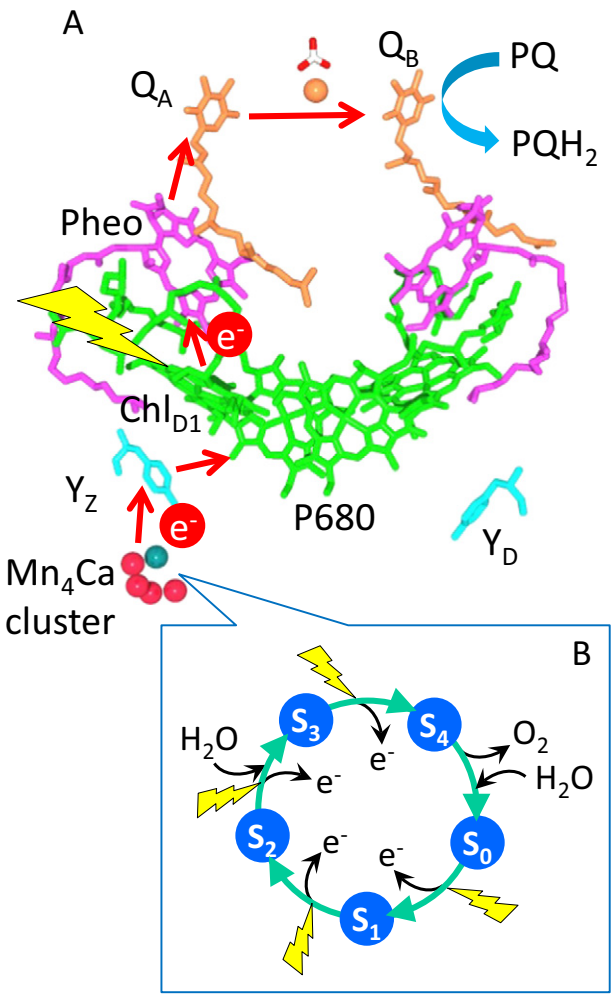

Fig. 1. (A) Arrangements of redox cofactors in photosystem II and the electron transfer pathway. (B) S-state cycle of water oxidation at the Mn_4CaO_5 cluster.

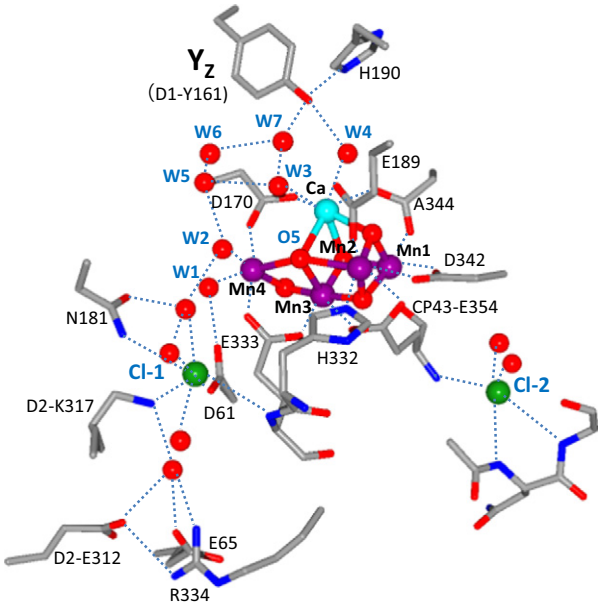

Fig. 2. Structure of WOC deduced from the X-ray crystal structure of photosystem II at 1.9 Å resolution (PDB ID: 3ARC [14]). Amino acid residues in which the subunit name is not specified in the labels are all on the D1 subunit. The numbering of the atoms in the Mn_4CaO_5 cluster, Cl^- ions, and water molecules follows that of Umena et al. [14] and Kawakami et al. [128].

were ligated to Mn4, and W3 and W4 were ligated to Ca (the numbering follows Umena et al. [14]). In addition to these four water molecules, the oxygen atom O5, which is located nearly equidistant from Ca, Mn4, Mn3 and Mn1 in the Mn_4CaO_5 cluster, is a possible candidate substrate [14–16]. Hydrogen bond networks involving these water ligands are formed around the Mn_4CaO_5 cluster. In particular, a water cluster consisting of W3, W4, W5, W6 and W7 is present between the Mn_4CaO_5 cluster and Y_Z, whereas a hydrogen bond network involving D1-Asp61, D2-Lys-317, D1-Glu65, D2-Glu312, D1-Arg334 and several water molecules is formed around one of the Cl^- ions (Cl-1) (Fig. 2). Such hydrogen bond networks likely play a crucial role in proton release processes during water oxidation.

At the WOC, two water molecules are oxidized into one O_2 molecule and four protons through the cycle of five intermediates designated S_i states ($i = 0$–4); a larger i value implies a higher oxidation state of the Mn_4CaO_5 cluster (Fig. 1B) [1–8]. The S_1 state is most stable in the dark, and the S_i state ($i = 0$–3) advances to the next S_{i+1} state upon the extraction of one electron. The S_4 state is a transient intermediate that immediately relaxes to the S_0 state by releasing O_2. However, there are several unanswered questions in the water oxidation mechanism. For example, it remains unclear how the electron and proton transfer reactions are coupled with each other in individual S-state transitions. It is also unknown in which order the electron and protons are released from the WOC. Similarly, the pathway in the PSII proteins for the release of each proton and the energetic requirement that drives the reaction are yet to be elucidated. Answering these questions is essential to achieve a full understanding of the mechanism of photosynthetic water oxidation.

Infrared (IR) spectroscopy, particularly light-induced Fourier transform infrared (FTIR) difference spectroscopy [17–19], has been used extensively to study the mechanism of photosynthetic water oxidation [20–28]. Flash-induced FTIR difference spectra have been measured upon individual transitions in the S-state cycle ($S_1 \rightarrow S_2$, $S_2 \rightarrow S_3$, $S_3 \rightarrow S_0$ and $S_0 \rightarrow S_1$) [29,30], and data regarding the structures and reactions of the proteins and water molecules during water oxidation have been obtained. Time-resolved infrared (TRIR) spectroscopy was also used to monitor the movements of electrons and protons *during* the S-state transitions of WOC reaction [31]. In this review, I summarize the applications of light-induced FTIR difference and TRIR spectroscopies for investigating the molecular mechanism of photosynthetic water oxidation, focusing on the coupling of electron and proton transfer reactions. For other topics, such as ligand structure, water reactions, lower-frequency Mn cluster vibrations, and the effects of extrinsic proteins, I refer readers to previous reviews [20–28].

2. Flash-induced FTIR difference spectra of the S-state transitions

Fig. 3 shows flash-induced FTIR difference spectra of the S-state transitions measured using PSII core complexes from the cyanobacterium *Thermosynechococcus elongatus* in the presence of ferricyanide as an exogenous electron acceptor [29,32,33]. Because electrons are abstracted by ferricyanide to the outside of proteins, IR changes coupled to the WOC reactions are obtained without interference from acceptor side signals, except for the CN stretching vibrations of ferricyanide/ferrocyanide at 2116/2038 cm^{-1}. Difference spectra upon the 1st, 2nd, 3rd and 4th flashes virtually represent structural changes in the $S_1 \rightarrow S_2$, $S_2 \rightarrow S_3$, $S_3 \rightarrow S_0$ and $S_0 \rightarrow S_1$ transitions, respectively, although minor contributions of other transitions are mixed into the spectra at the later flashes due to ~10% miss probabilities (see Section 3).

Numerous signals are found in the mid-frequency region of 1800–1000 cm^{-1}, where protein bands mainly appear [34,35], which is indicative of drastic protein movements during water oxidation. The presence of several prominent bands in the amide I (the CO stretch of backbone amide) region at 1700–1600 cm^{-1} indicates that the

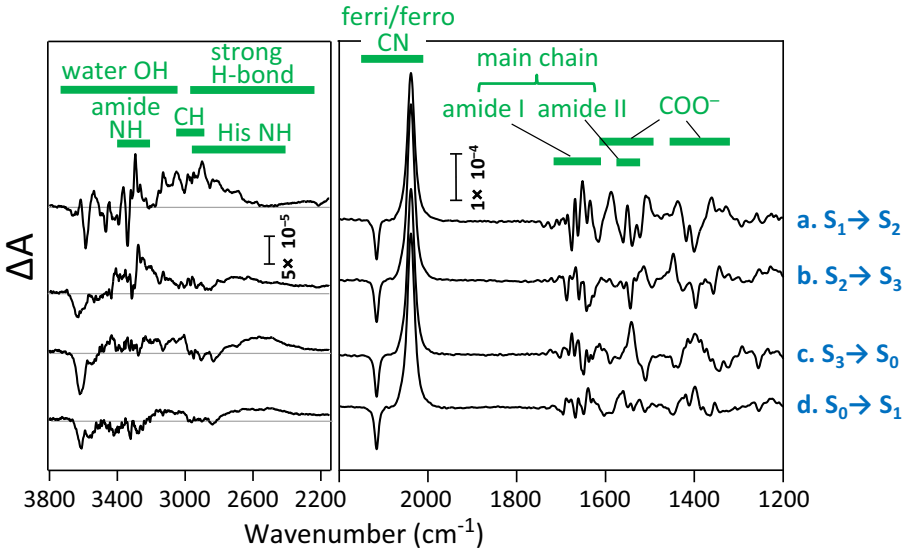

Fig. 3. Flash-induced FTIR difference spectra in the high-frequency (3800–2200 cm^{-1}) and mid-frequency (2200–1200 cm^{-1}) regions during the S-state cycle of WOC in the PSII core complexes from *T. elongatus* [33]. Difference spectra upon the first (a), second (b), third (c), and fourth (d) flashes represent the changes in the $S_1 \rightarrow S_2$, $S_2 \rightarrow S_3$, $S_3 \rightarrow S_0$, and $S_0 \rightarrow S_1$ transitions, respectively.

secondary structures of the proteins around the Mn_4CaO_5 cluster are affected significantly by the S-state transitions. These amide I features have been used to assess the effects of binding of extrinsic proteins on the conformation of proteins in the WOC [36–40]. Significant bands also appear in the region of 1600–1500 cm^{-1}, where the amide II (the NH bend coupled to the CN stretch of backbone amide) and asymmetric COO^- stretching bands overlap [34,35]. Essentially, all of the prominent bands in the 1450–1300 cm^{-1} region arise from the symmetric COO^- stretching vibrations of carboxylate groups coupled to the Mn_4CaO_5 cluster [34,35,41]. Spectra were analyzed using site-directed mutants of putative carboxylate ligands and/or isotopic substitutions [42–54]. Among these, the bands of D1-Ala344 (α-COO^-) [42–45] and CP43-Glu354 [46–48] were identified successfully at 1360–1320 and 1435–1390 cm^{-1}, respectively. The carboxylate bands are also sensitive to perturbations of the Mn_4CaO_5 cluster including Ca depletion and Sr substitution [41,43,55–57], as well as to various treatments such as NH_3/NH_4^+ treatment [58–61] and replacing Cl^- with other anions [62,63].

His CN stretching bands are detected at ~1110 cm^{-1} [64,65], due probably to D1-His332, which is ligated to Mn2, and possibly to D1-His337, which interacts with O3. Selective isotope labeling of Arg side chains identified CN/NH_2 vibrations from Arg, most probably CP43-Arg357 that is located in the vicinity of the Mn_4CaO_5 cluster, in the 1700–1600 cm^{-1} region overlapping with the amide I bands in the S_2/S_1 difference spectrum. This provides evidence for the structural coupling of this Arg with the Mn_4CaO_5 cluster and the existence of fully protonated guanidinium form in both the S_1 and S_2 states [66].

Stretching vibrations of hydrogen atoms such as water OH, amide NH, and hydrocarbon CH appear in the higher-frequency region of 3700–2200 cm^{-1} (Fig. 3) [33]. In particular, relatively narrow bands in the region of 3700–3500 cm^{-1} represent the vibrations of weakly hydrogen-bonded OH bonds of water molecules coupled to the Mn_4CaO_5 cluster, probably involving substrate water [25,33,60,67,68]. The differential signal at 3617/3588 cm^{-1} in the $S_1 \rightarrow S_2$ transition suggests a change in the hydrogen bond strength of a water ligand. In contrast, the negative intensities of bands at 3634, 3621, and 3612 cm^{-1} in the $S_2 \rightarrow S_3$, $S_3 \rightarrow S_0$, and $S_0 \rightarrow S_1$ transitions, respectively, imply the disappearance of weakly hydrogen-bonded OH bonds, either by the release of the proton or by a change from a weak to strong hydrogen bond [25,33,67]. Very broad features in the 3000–2200 cm^{-1} region, which have different positions of the maxima (at ~3000, ~2700, ~2550 and ~2600 cm^{-1} in the $S_1 \rightarrow S_2$, $S_2 \rightarrow S_3$, $S_3 \rightarrow S_0$ and $S_0 \rightarrow S_1$ transitions, respectively) have been attributed to the vibrations of polarizable protons in the strong hydrogen bonds around the Mn_4CaO_5 cluster [33,68]. The shifts in the band positions indicate changes in the hydrogen bond network around the Mn_4CaO_5 cluster during the S-state transitions. Several peaks on the broad feature at 3000–2500 cm^{-1} arise from the Fermi resonance of His vibrations with its NH stretching vibration [64]. Although Polander and Barry [69] recently assigned a positive band at 2880 cm^{-1} in the S_2/S_1 difference spectrum to a cationic cluster of internal water molecules, this band was downshifted by ^{15}N and ^{13}C substitutions, but unchanged by $H_2^{18}O$ substitution (Fig. S5 in ref. [70]); therefore, it could probably be attributed to the Fermi resonance of a His side chain. Although the broad feature might arise from the hydrogen bond network involving a water cluster located between the Mn_4CaO_5 cluster and Y_Z, there is no experimental evidence to date to suggest that a cation is formed in the water cluster upon S_2 formation, and no quantum chemical calculations predict the formation of cationic water during the $S_1 \rightarrow S_2$ transition (e.g., [15,71]). A recent FTIR study of the D1-Asp61Ala mutant by Debus [68] revealed that the hydrogen bond network that causes the broad feature of the S_2/S_1 difference spectrum involves D1-Asp61.

Water vibrations were also detected as DOD bending vibrations at ~1200 cm^{-1} using PSII in D_2O [68,72], which was used instead of H_2O to avoid severe overlap of the HOH bending vibration (~1640 cm^{-1}) with the amide I bands of the proteins. DOD bending bands coupled to the S-state transitions were observed at 1250–1150 cm^{-1} in ^{16}O-minus-^{18}O double difference spectra. The involvement of several water molecules in the reaction cycle and the insertion of substrate water into WOC during the $S_2 \rightarrow S_3$ and $S_3 \rightarrow S_0$ transitions were revealed [72]. These water insertion steps are consistent with the FTIR observation that the efficiency of the S-state transition is lowered by dehydration more significantly in the $S_2 \rightarrow S_3$ and $S_3 \rightarrow S_0$ transitions than in the $S_1 \rightarrow S_2$ and $S_0 \rightarrow S_1$ transitions [25,32]. However, the insertion of water in the $S_2 \rightarrow S_3$ transition is contradictory to membrane-inlet mass spectrometry (MIMS) data, which showed that both substrate water molecules are already bound in the S_2 state (summarized in the recent review [8]). Therefore, it is likely that the water molecule inserted into the WOC during the $S_2 \rightarrow S_3$ transition functions as a substrate in the next cycle. The recent analysis of the DOD bending bands of a D1-Asp61Ala mutant suggested that D1-Asp61 forms a hydrogen bond with a water molecule that is affected by the $S_1 \rightarrow S_2$ transition [68].

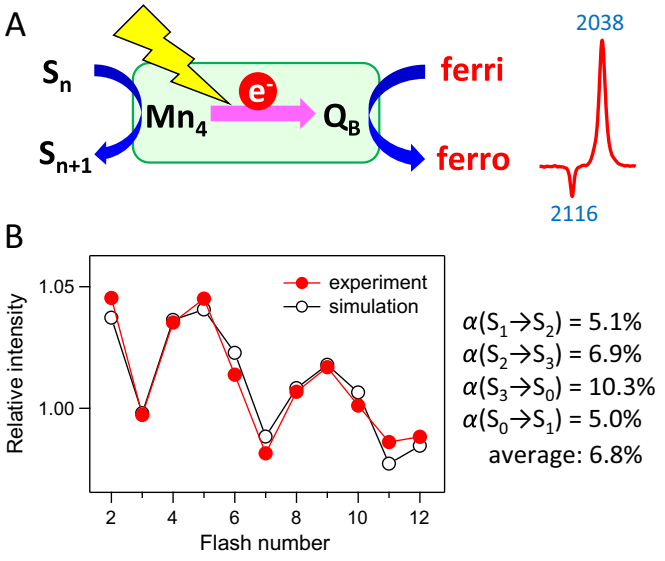

Fig. 4. (A) Schematic view of monitoring the electron flow in photosystem II using FTIR signals of the ferricyanide/ferrocyanide redox couple. (B) Flash-number dependence of the intensity of the ferricyanide/ferrocyanide signal (red solid circles) with the result of simulation (black open circles) to provide miss probabilities of individual S-state transitions [77].

3. FTIR detection of electron transfer from WOC to the acceptor side: estimation of the efficiencies of individual S-state transitions

Electron transfer reactions of WOC can be monitored using the strong CN stretching bands of ferricyanide/ferrocyanide at 2116/2038 cm^{-1} in the flash-induced FTIR difference spectra of the S-state transitions (Fig. 3). The intensity of this signal reflects how efficiently an electron is transferred from the WOC to the electron acceptor side and finally to ferricyanide at each flash (Fig. 4A). This eventually reflects the advancement of the individual S-states to the next state. The probability that the S-state transition fails to advance is called a "miss". Misses in the S-state transitions are thought to arise from charge recombination between $P680^+$ and Q_A^- [73], and individual S-state transitions should have different miss probabilities because of the different kinetics and energetics of the S_i ($i = 0$–3) ↔ Y_Z ↔ P680 equilibrium (a detailed discussion of S-state dependent miss probabilities is found in [74]). Estimating the miss probabilities of individual transitions is crucial for detailed analysis of spectroscopic data as well as for understanding the water oxidation mechanism. However, only the average miss of the four transitions ($S_1 \rightarrow S_2$, $S_2 \rightarrow S_3$, $S_3 \rightarrow S_0$, and $S_0 \rightarrow S_1$) can be estimated using conventional methods such as the analysis of the flash-induced pattern of O_2 release [75], UV absorption [76] and FTIR protein signals [29,30].

To estimate the individual miss probabilities, the method needs to provide either (1) a common signal representing the advancement of S-state transitions irrespective of the transitions, or (2) different signals for individual S-state transitions but with known standard intensities. The former requirement was met by a novel FTIR method that could be used to estimate the individual miss probabilities [77]. Specifically, the intensity of the ferricyanide/ferrocyanide CN signal, which is common for all transitions, was monitored as a function of the flash number (Fig. 4B). This method is valid because, in the presence of ferricyanide, quinone electron acceptors, Q_A and Q_B, are always stabilized in their oxidized forms; therefore, there is virtually no effect of the $Q_A^-Q_B \leftrightarrow Q_AQ_B^-$ equilibrium on the miss probabilities of WOC. Thus, the original properties of the S-state transitions in WOC can be estimated independent from the acceptor side status. The first-flash data were not used in the analysis because non-heme iron preoxidized in some centers accepts an electron that is released by the first flash. Simulating the oscillation pattern of the flash number-dependence of the signal amplitude provided the miss probabilities of the individual transitions without making any assumptions. The general tendency of misses was found to be in the order of $S_0 \rightarrow S_1 \leq S_1 \rightarrow S_2 < S_2 \rightarrow S_3 < S_3 \rightarrow S_0$, suggesting that more oxidized WOC has a higher miss probability [77]. This tendency was consistent with the estimation in the fluorescence study by de Wijn and van Gorkom [78], which, however, required some assumptions in parameters related to fluorescence and a miss contribution associated with Q_B^-. It was presumed that the higher oxidation state of the Mn_4CaO_5 cluster shifted the electron transfer equilibrium of WOC ↔ Y_Z ↔ P680 to the P680 side [77,78]. The largest miss in the $S_3 \rightarrow S_0$ transition is also consistent with a significant portion of microsecond components in the $P680^+$ reduction kinetics in the $S_3 \rightarrow S_0$ transition [79] as well as the presence of an ~200 μs "lag phase" before electron transfer from WOC to $Y_Z^\bullet$ (see Section 5) [31,80,81]. In contrast to the FTIR and fluorescence estimations, an EPR study performed by Han et al. [82], in which signals specific to individual S states were used, provided a rather different trend of miss probabilities with a relatively low miss in the $S_3 \rightarrow S_0$ transition. The reason for this discrepancy is unknown, although the difference in exogenous electron acceptors [ferricyanide in FTIR vs. phenyl-*p*-benzoquinone (*p*BQ) in EPR] could play a role.

4. FTIR detection of proton release from WOC: estimation of the proton release pattern

The conventional methods used to monitor proton release from WOC and estimate its stoichiometry in individual S-state transitions involved detecting flash-induced pH changes using pH-indicating dyes or a sensitive pH electrode [83–88]. These methods used buffers at very low concentrations to detect small shifts in pH. However, there is a concern that the protons released from the WOC are trapped by PSII proteins that possess a large number of protonatable groups in such low concentration buffers. Suzuki et al. [89] developed a novel method for detecting proton release using FTIR difference spectroscopy. In this method, PSII core samples were suspended in a high concentration (200 mM) Mes buffer, and the protons released from the WOC upon flash illumination were trapped by the buffer molecules. The protonation reaction in the Mes buffer was then monitored using FTIR difference spectroscopy, and isotope-edited Mes signals without protein contributions were obtained from a double difference spectrum between unlabeled and d_{12}-labeled Mes (Fig. 5A). The flash number-dependence of the intensity of the isotope-edited Mes signal showed a clear period-four oscillation (Fig. 5B). The simulation of this oscillation provided the proton release pattern of 0.8–1.0 ($S_0 \rightarrow S_1$):0.2–0.3 ($S_1 \rightarrow S_2$):0.9–1.2 ($S_2 \rightarrow S_3$):1.5–1.6 ($S_3 \rightarrow S_0$) [89]. This pattern is consistent with the proton release of 1:0:1:2 from substrate water (Fig. 5C), while deviations from the integer values were ascribed to the partial protonation/deprotonation reactions of amino acid side chains near the WOC [83,87–89].

This proton release pattern is also consistent with the pH-dependence of the S-state transition efficiencies estimated using FTIR spectroscopy [90]. The efficiency of the $S_1 \rightarrow S_2$ transition was independent of pH values within the range 3.5–9.5, whereas the other three transitions were all inhibited at acidic pHs with pK_a values of 3.6, 4.2 and 4.7 for the $S_2 \rightarrow S_3$, $S_3 \rightarrow S_0$ and $S_0 \rightarrow S_1$ transitions, respectively. A similar pH dependence in the acidic pH region was also observed using EPR spectroscopy [91]. The observed low pH inhibition in the $S_2 \rightarrow S_3$, $S_3 \rightarrow S_0$ and $S_0 \rightarrow S_1$ transitions was explained by proton release from substrate water at these three transitions [90].

The above proton release pattern together with the abstraction of a single electron by $Y_Z^\bullet$ in each S-state transition implies that an excess positive charge accumulates on the Mn_4CaO_5 cluster in the S_2 and S_3 states (Fig. 5C). This excess positive charge might play a key role in the mechanism of proton-coupled electron transfer (PCET) at the S_2 and S_3 states as discussed in Sections 5 and 6 below [6,31,80,81,92].

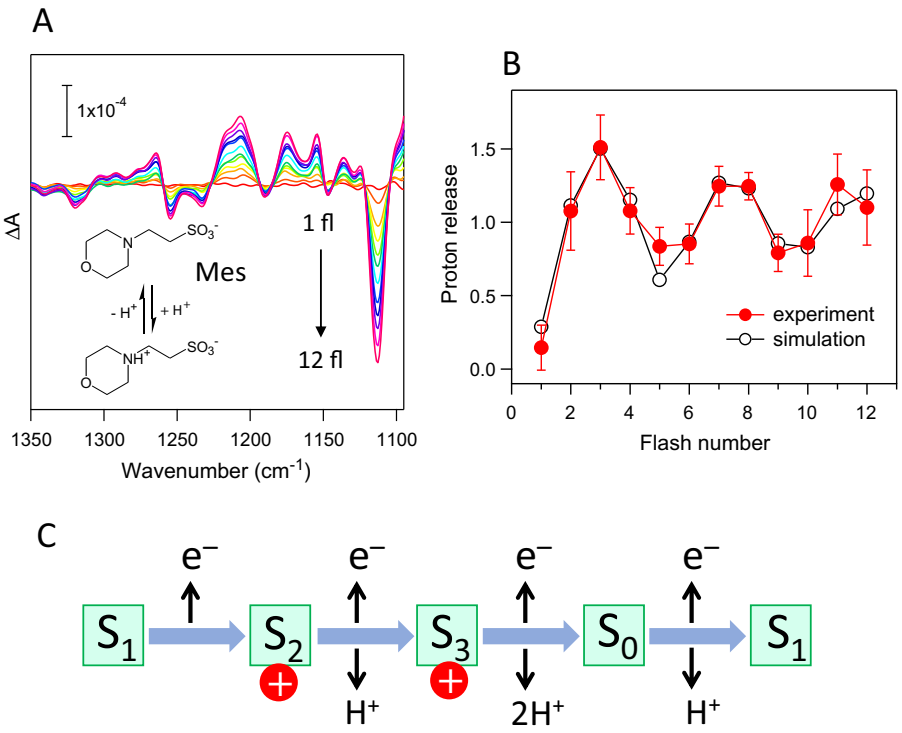

Fig. 5. (A) Detection of proton release from WOC using the isotope-edited bands of a Mes buffer. Mes-*minus*-Mes-d_{12} double difference spectra were obtained from FTIR difference spectra upon flash illumination (1–12 flashes) on the PSII core complexes of *T. elongatus* in 200 mM Mes (unlabeled and d_{12}-labeled) buffer [89]. (B) Proton release pattern as a function of the flash number estimated from the Mes signals (red solid circles) together with a simulated pattern (black open circles). (C) Proton release stoichiometry during the S-state cycle estimated from FTIR. This stoichiometry together with electron abstraction at each transition implies that an excess positive charge resides on the Mn_4CaO_5 cluster at the S_2 and S_3 states.

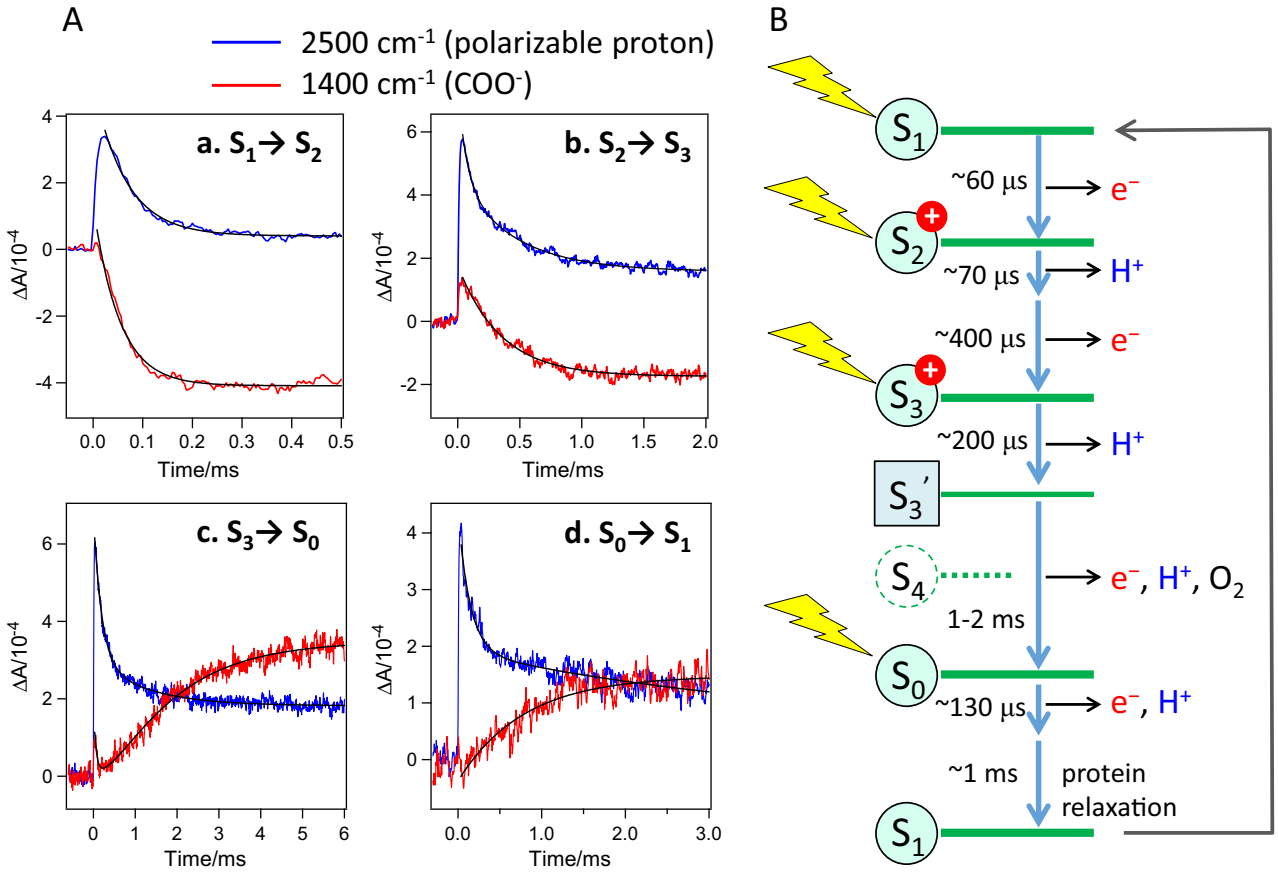

Fig. 6. (A) Time courses of the infrared signal at 2500 (blue line) and 1400 (red lines) cm^{-1} during the $S_1 \rightarrow S_2$ (a), $S_2 \rightarrow S_3$ (b), $S_3 \rightarrow S_0$ (c), and $S_0 \rightarrow S_1$ (d) transitions of the S-state cycle [31]. (B) Proton-coupled electron transfer processes in the S-state cycle proposed from the TRIR results.

5. Detecting proton-coupled electron transfer: time-resolved infrared measurements

Although flash-induced FTIR difference spectroscopy has provided various pieces of information about the reactions of WOC, it can detect only structural changes between the relaxed states of stable or metastable intermediates (S_0, S_1, S_2, and S_3). To obtain information on PCET and the reactions of substrate and proteins *during* the S-state transitions, Noguchi et al. [31] applied time-resolved IR (TRIR) spectroscopy to water oxidation studies. They used the dispersive-type TRIR method, rather than the step-scan FTIR method that has been used extensively in other biological systems such as bacteriorhodopsin [93–95], because a fast repetition rate, which is prerequisite for the step-scan method, is rather limited in the S-state cycles. The wavenumbers of 1400 and 2500 cm^{-1}, which represent vibrations of the carboxylate groups and polarizable protons in strong hydrogen bonds (see Section 2), respectively, were used to monitor the WOC reactions. The absorbance change at 1400 cm^{-1} reveals perturbations of the carboxylate ligands that are triggered by the redox change of Mn ions or the carboxylate groups coupled to the Mn_4CaO_5 cluster through a hydrogen bond network including protonation/deprotonation reactions in proton pathways. In addition, the change at 2500 cm^{-1} reveals the movement or changes in the interactions of protons in hydrogen bond networks within the protein as well as proton release.

Individual S-state transitions exhibited characteristic behaviors in the time courses of the absorption changes at 1400 and 2500 cm^{-1} (Fig. 6A) [31]. At 1400 cm^{-1} (red lines), the time courses converge into negative amplitudes in the $S_1 \rightarrow S_2$ and $S_2 \rightarrow S_3$ transitions, whereas they converge into positive amplitudes in the $S_3 \rightarrow S_0$ and $S_0 \rightarrow S_1$ transitions. This is consistent with the observation that the S_2/S_1 and S_3/S_2 FTIR difference spectra had negative intensities, whereas the S_0/S_3 and S_1/S_0 spectra exhibited positive intensities around 1400 cm^{-1} (Fig. 3) [29,30]. At 2500 cm^{-1}, all the time courses had initial positive intensities, with subsequent relaxation. These initial positive intensities include contributions from the polarizable proton between Y_Z• and D1-His190 trapped as $HisH^+$ (see Section 6.2) [70], as well as hydrogen bond networks around the Mn_4CaO_5 cluster. During the $S_1 \rightarrow S_2$ transition, both wavenumbers showed single exponential decays with time constants of 50–70 μs (Fig. 6Aa), which is consistent with the previously estimated time constant of the electron transfer from the Mn_4CaO_5 cluster to Y_Z• [80,81]. Because there is no proton release during this transition, this observation indicates that the rearrangement of protons in the hydrogen bond networks is concerted with the electron transfer. For the $S_2 \rightarrow S_3$ transition, a time constant of ~350 μs was obtained from the single exponential decay at 1400 cm^{-1}, whereas the decay curve at 2500 cm^{-1} clearly showed two phases with fast (τ ~70 μs) and slow (τ ~460 μs) time constants (Fig. 6Ab). Because this slow phase at 300–500 μs was consistent with the previously reported rate of electron transfer during this transition [80,81], the 70 μs phase was interpreted as reflecting the rearrangement of protons in the hydrogen bonds in proteins or even proton release to the bulk. This TRIR result suggests that proton transfer precedes electron transfer in the $S_2 \rightarrow S_3$ transition, although the faster phase was not resolved clearly at 1400 cm^{-1}. The rapid proton release before electron transfer during the $S_2 \rightarrow S_3$ transition was also proposed recently from a photothermal beam deflection experiment, in which an ~30-μs component was detected during this transition [92].

For the $S_3 \rightarrow S_0$ transition, the presence of a distinct intermediate, S_3' (distinguished from the S_4 state having an oxidized catalytic center), and a "lag phase" ($S_3 \rightarrow S_3'$, ~200 μs) before the electron transfer from the Mn_4CaO_5 cluster to Y_Z• was proposed from time-resolved UV and X-ray absorption measurements [80,81]. Although proton release was suggested to take place during this lag phase [80,81], there was no direct evidence for the presence of proton transfer. The change in IR absorption at 1400 cm^{-1} exhibited a complex behavior with a fast decay phase (τ ~60 μs) followed by a slow, sigmoidal-shaped rise (τ ~1.6 ms) (Fig. 6Ac) [31]. This sigmoidal rise reflects the presence of a "lag phase" before the electron transfer. Significantly, the time course at 2500 cm^{-1} exhibited a drastic IR change in a relatively fast phase with a time constant of ~190 μs, which is consistent with the ~200 μs "lag phase" [80,81]. This early phase was followed by a slow phase (τ ~1.2 ms) corresponding to the ~1.6-ms phase at 1400 cm^{-1} (Fig. 6Ac), representing electron transfer. Therefore, the TRIR measurements provided the first experimental evidence that drastic proton rearrangement, probably proton release from substrate water, occurs during the "lag phase" before electron transfer [31]. The slow (τ = 1–2 ms) electron transfer drives the Mn_4CaO_5 cluster to the S_4 state, which immediately relaxes to the S_0 state by releasing another proton and O_2. The fast ~60 μs decay phase in the carboxylate movements could be related to the protein rearrangement upon Y_Z• formation that has been observed at 30–40 μs [96].

During the $S_0 \rightarrow S_1$ transition, the time course at 2500 cm^{-1} exhibited a major phase with a relatively fast rate (τ ~130 μs) followed by a minor slow decay (τ = 1–4 ms), whereas that at 1400 cm^{-1} exhibited a single exponential rise with a relatively slow rate (τ ~800 μs) (Fig. 6Ad) [31]. Because the electron transfer in this transition has been estimated to be relatively fast (30–250 μs) [80,81], the faster 130 μs phase at 2500 cm^{-1} was assigned to electron transfer coupled with proton transfer [31]. The much slower carboxylate change (~800 μs) at 1400 cm^{-1} together with the minor proton decay (τ = 1–4 ms) at 2500 cm^{-1} was proposed to reflect the relaxation of the protein conformation after electron transfer, which could contribute to stabilizing the S_1 state relative to other S states [31].

The electron and proton transfer processes suggested from the TRIR results are summarized in Fig. 6B. The $S_1 \rightarrow S_2$ transition is a simple process of concerted PCET between Y_Z and the Mn_4CaO_5 cluster with a time constant of ~60 μs. The proton on D1-His190, which provides a positive intensity at ~2500 cm^{-1}, returns to Y_Z• upon its rereduction by the Mn_4CaO_5 cluster. An early deprotonation process observed during the $S_3 \rightarrow S_0$ transition, and most likely during the $S_2 \rightarrow S_3$ transition, is a crucial step for lowering the redox potential of the Mn_4CaO_5 cluster, which possesses an excess positive charge in the S_2 and S_3 states (see Section 4), to facilitate its oxidation [80,81,92]. In particular, a drastic proton movement in the "lag phase" for ~200 μs before electron transfer, which most provably indicates the release of a proton from the substrate, was detected clearly. The $S_0 \rightarrow S_1$ transition might be a concerted PCET reaction, in which a proton is released from substrate water concomitant with electron transfer. This process seems to be followed by a slow conformational change of the proteins, relaxing to the dark stable S_1 state. These TRIR-detected proton and electron transfer processes and the estimated time constants are mostly consistent with those proposed by other spectroscopic methods, such as time-resolved X-ray absorption and UV absorption [80,81,92]. However, the rate of electron transfer during the $S_0 \rightarrow S_1$ transition (~130 μs) is much slower than that recorded using X-ray absorption (30 μs) [81], and Klauss et al. [92] suggested recently that proton transfer occurs after electron transfer in this transition. In addition, an intermediate formed during the $S_2 \rightarrow S_3$ transition by proton transfer before electron transfer was not identified clearly by the TRIR measurements. Therefore, additional careful TRIR studies using various samples and with better time resolutions are necessary to reach a definitive conclusion regarding the mechanism of PCET during water oxidation.

6. FTIR analysis of proton release pathways

Another unknown aspect of the water oxidation mechanism is the pathways of release of protons from substrate water. Because proton release occurs in three transitions ($S_2 \rightarrow S_3$, $S_3 \rightarrow S_0$ and $S_0 \rightarrow S_1$; see Section 4), it remains unclear whether only a single pathway is used for all of the four protons, or whether different pathways are used for individual protons. Possible proton pathways have been predicted [14,97–102] using information obtained from the X-ray crystallographic

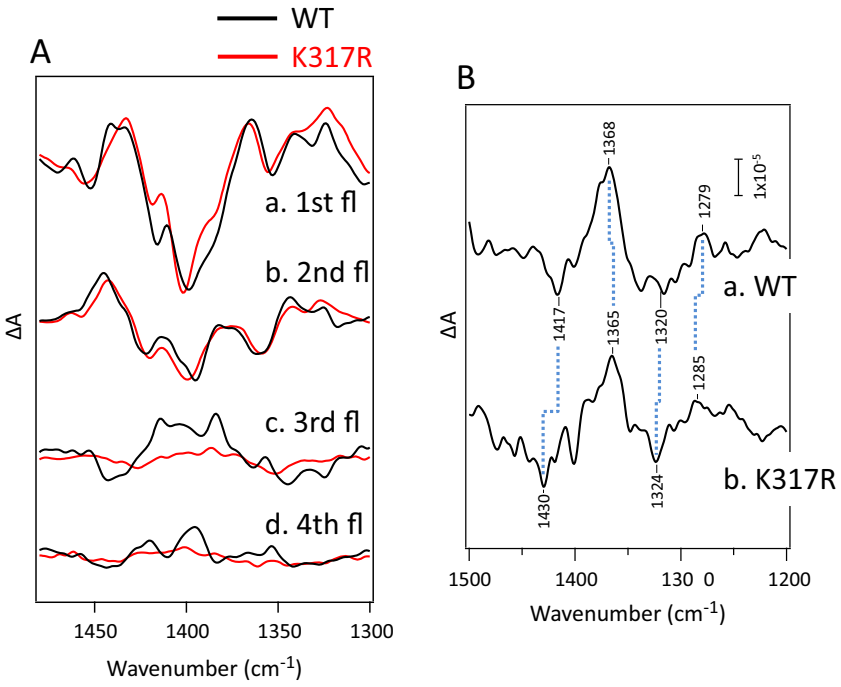

Fig. 7. (A) FTIR difference spectra of the S-state cycle in the moderately hydrated films of PSII complexes from WT (black lines) and the D2-K317R mutant (red lines) of *Synechocystis* sp. PCC 6803 upon illumination of the 1st (a), 2nd (b), 3rd (c), and 4th (d) flashes [107]. (B) $^{14}NO_3^-$-minus-$^{15}NO_3^-$ double difference spectra of the S_2/S_1 difference spectra measured with the NO_3^--treated PSII complexes of WT (a) and D2-K317R (b).

structures of PSII protein complexes [12–14]. In particular, the recent high-resolution (1.9 Å) structure [14] that resolved the positions of oxygen atoms in water molecules revealed hydrogen bond networks as candidates of proton pathways. Among the several proposed pathways, the most focused is that in which the hydrogen bond network starts from D1-Asp61 and passes through Cl-1 to the thylakoid lumen [68,100,103–111]. Another suggested pathway is a hydrogen bond network connecting Y_Z to the lumen [14,70,99]. FTIR difference spectroscopy has been used to investigate the involvement of these hydrogen bond networks, as well as the roles of the Cl^- site and Y_Z in the proton transfer mechanism of water oxidation [68,70,107,108,112,113].

6.1. Pathway via Cl-1

The WOC reactions of site-directed mutants at D2-Lys317, which is a ligand to Cl-1, were examined using light-induced FTIR difference spectroscopy [107,108]. Pokhrel et al. [108] measured the FTIR difference spectra of the S-state cycle together with the EPR spectra and O_2-release kinetics for several mutants, including D2-Lys317Arg and D2-Lys317Ala. They showed that the S-state transitions, particularly, the $S_3 \rightarrow S_0$ transition, are less efficient in these mutants. Suzuki et al. [107] also demonstrated that the $S_3 \rightarrow S_0$ transition is blocked in partially dehydrated film of the PSII core complexes from the D2-Lys317Arg mutant (Fig. 7A). This mutation also exhibited altered ^{15}N isotope-edited NO_3^- bands in the spectrum of PSII in which Cl^- is replaced with NO_3^- (Fig. 7B), suggesting that the Cl-1 site is coupled structurally to the Mn_4CaO_5 cluster. In addition, FTIR studies by Debus and coworkers [68,112,113] revealed that mutating D1-Asp61, D1-Glu65, D2-Glu312 and D1-Arg334, which interact with the Cl-1 site through a hydrogen bond network (Fig. 2), to Ala decreased the $S_3 \rightarrow S_0$ efficiency substantially and altered the C=O stretching band of protonated carboxylic acid at 1746 cm^{-1}. These data suggest that the Cl-1 site, nearby protonatable amino acids, and surrounding water molecules are involved in the proton transfer pathway during the $S_3 \rightarrow S_0$ transition. An attractive mechanism is that the structure of the Cl-1 site is regulated by the redox status of the Mn_4CaO_5 cluster, and that the "gate" is opened for proton transfer during the $S_3 \rightarrow S_0$ transition [107].

These observations and hypotheses are consistent with the increase in the miss probability at the $S_3 \rightarrow S_0$ transition when Cl^- was replaced with NO_3^-, which was detected by the FTIR method using ferricyanide/ferrocyanide bands (see Section 2) [77]. A time-resolved UV absorption study also showed that replacing Cl^- with other functional monovalent ions such as NO_3^- and I^- reduced the rate of the $S_3 \rightarrow S_0$ transition [113–116]. In contrast, the efficiency of the $S_2 \rightarrow S_3$ transition was not affected significantly by the D1-Asp61Asn and D2-Lys317Arg mutants [107,108,110,111], and the $S_0 \rightarrow S_1$ transition was also unaffected by Cl^- depletion [117]. Therefore, it is likely that the Cl-1 pathway is not used to release protons during the $S_2 \rightarrow S_3$ and $S_0 \rightarrow S_1$ transitions.

6.2. Pathway via Y_Z

When Y_Z is oxidized by $P680^+$, the phenolic proton is released resulting in the formation of a neutral Y_Z• radical [5,118–122]. Although another redox-active Tyr on the D2 subunit, Y_D (D2-Tyr160), is also oxidized by $P680^+$ to become a neutral Y_D• radical, its reaction rate is considerably slower than that of Y_Z. In addition, Y_D• is significantly stable even at room temperature, in contrast to the short lifetime of Y_Z• [5,118,119]. Berthomieu et al. [123] first reported the FTIR difference spectrum of Y_Z upon its photo-oxidation (Y_Z•/Y_Z difference) in the 1800–1000 cm^{-1} region using Mn-depleted PSII preparations. They observed a higher νCO frequency in Y_Z• (1514 cm^{-1}) than in Y_D• (1504 cm^{-1}), and proposed the presence of a stronger hydrogen bond in Y_Z• compared with Y_D•. Theoretical calculations also suggested that a stronger hydrogen bond upshifts the νCO frequency of the Tyr• radical [124,125].

Recently, Nakamura et al. [70] measured Y_Z•/Y_Z spectra including the higher frequency region that involves proton vibrations. The spectrum exhibited a broad positive feature around 2800 cm^{-1} (Fig. 8A), which was absent from the Y_D•/Y_D difference spectrum. Measurements using ^{15}N-substituted and H/D-exchanged PSII samples and vibrational analyses using density functional theory (DFT) and quantum mechanics/molecular mechanics (QM/MM) calculations showed that this band arises from the N – H stretching vibration of the protonated cation of D1-His190, which is formed by accepting a proton from Y_Z and forms a strong hydrogen bond with Y_Z•. The broad feature of the ~2800 cm^{-1}

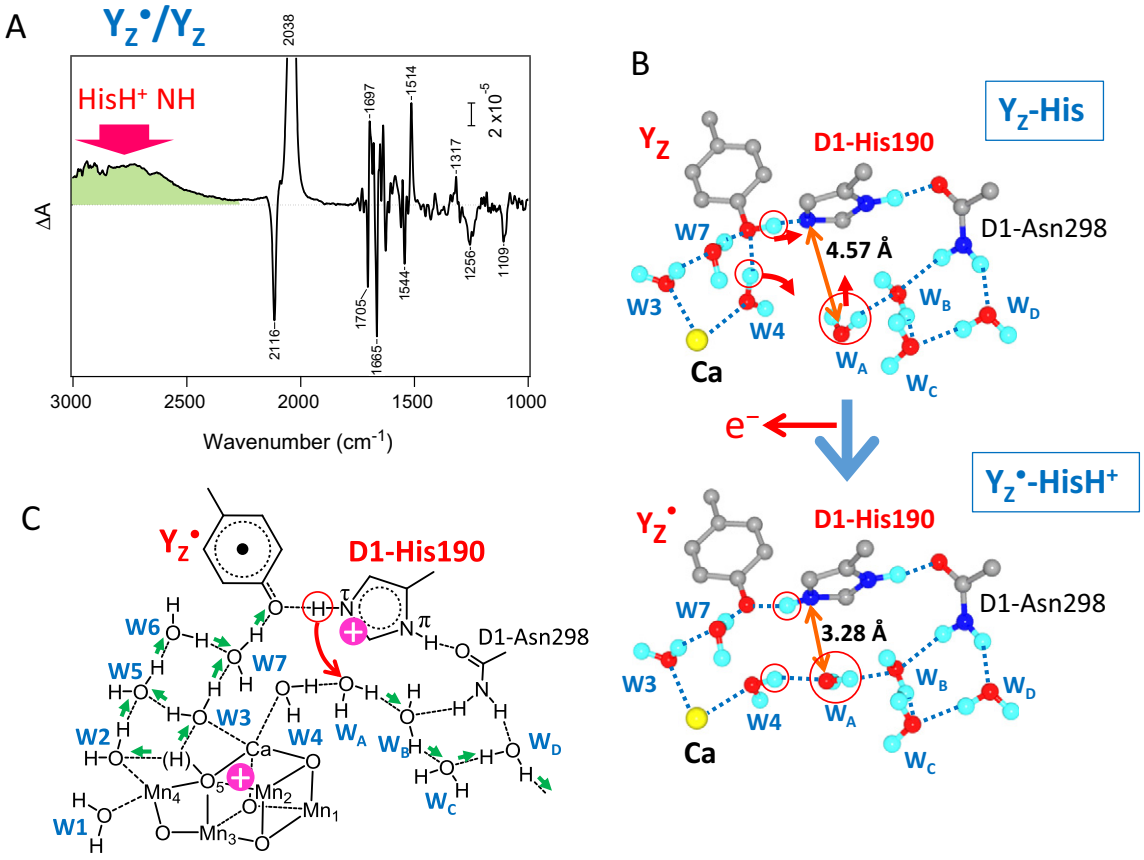

Fig. 8. (A) A light-induced $Y_Z^•/Y_Z$ FTIR difference spectrum (3000–1000 cm^{-1}) of the PSII core complexes from *T. elongatus* [70]. (B) Rearrangement of the hydrogen bond network near Y_Z upon its oxidation estimated by QM/MM calculations. The drastic movements of protons and a water molecule are expressed with red circles and red arrows. (C) Proposed proton release mechanism from substrate water on the Mn_4CaO_5 cluster via the $Y_Z^•$-$HisH^+$ moiety as a 'gate'. Hopping of the polarizable proton (red circle) to W_A, which moved toward D1-His190 upon Y_Z oxidation (B), triggers immediate proton transfer from substrate water to Y_Z through the water cluster by the Grotthuss mechanism (green arrows).

band suggests that the proton trapped between $Y_Z^•$ and D1-His190 has a large polarizability. Therefore, this proton is movable in response to changes in the charge distribution of the Mn_4CaO_5 cluster as well as fluctuations of the protein and water environments.

The QM/MM calculations performed by Nakamura et al. [70] further exhibited a significant rearrangement of the hydrogen bond network around Y_Z, accompanied by the movement of water molecules upon Y_Z oxidation (Fig. 8B). The release of a proton from Y_Z, which results in the formation of a strong hydrogen bond with $HisH^+$, induces the breakage of the hydrogen bond between the W4 proton and Y_Z. This proton then turns to the direction of another water molecule (designated W_A; Fig. 8B). This rotation of W4 induces the movement of W_A toward D1-His190, which shortens the distance between the W_A oxygen and the N_τ of D1-His190 from 4.57 to 3.28 Å. Therefore, a network of water molecules is formed from W4 to W_D (Fig. 8B), which is further connected to the hydrogen bond network to the lumen [14].

A novel proton transfer mechanism via $Y_Z^•$-$HisH^+$ was proposed based on these FTIR observation and QM/MM data (Fig. 8C) [70]. Because the proton at the N_τ-H of D1-His190 is highly polarizable, there is a good chance that it is transferred to W_A, which is now located near this His. This proton hopping is the rate-limiting step that triggers rapid proton transfer from the water ligands, W4, W3 and W2 (and possibly O5, if this is a hydroxide [14]) as candidates of substrate water, to the Y_Z oxygen by the Grotthuss mechanism [126] (Fig. 8C). The proton accepted by W_A is transferred to the lumen via the network of the water molecules (W_A–W_D). Therefore, the rearrangement of the hydrogen bond network with the shift of a water molecule and the subsequent proton hopping from $HisH^+$ to this water are key events in the gating mechanism of proton transfer though Y_Z [70].

This type of proton transfer can occur in the S_2 or S_3 state, in which the electrostatic repulsion between the positive charge on $HisH^+$ and an excess positive charge on the Mn_4CaO_5 cluster drives proton release from substrate water before electron transfer to $Y_Z^•$ [31,80,81,92]. Because the $S_3 \rightarrow S_0$ transition appears to use the Cl-1 pathway (see Section 6.1), the $S_2 \rightarrow S_3$ transition is the primary candidate for transition using the $Y_Z^•$-$HisH^+$ pathway. This mechanism is also applicable to concerted PCET, in which proton and electron transfer between $Y_Z^•$ and the Mn_4CaO_5 cluster occurs simultaneously. If the $S_0 \rightarrow S_1$ transition has a concerted PCET mechanism, as suggested by the TRIR measurements (Fig. 6B: Section 5), it is possible that this transition also uses the $Y_Z^•$-$HisH^+$ pathway. This concerted mechanism differs from the previous "hydrogen abstraction model" [127], in which a proton from Y_Z is first released to the lumen upon its photo-oxidation, and then a hydrogen atom (or a proton and an electron) is abstracted by $Y_Z^•$ from the Mn_4CaO_5 cluster. In the newly proposed mechanism, proton transfer from $HisH^+$ as a triggering reaction determines the rate of the entire PCET process, and hence the deprotonated $Y_Z^•$-His is not formed as a stable intermediate. This PCET mechanism during the $S_0 \rightarrow S_1$ transition is also consistent with a previous suggestion by Renger [5], whereby $Y_Z^•$-induced oxidation steps in the WOC are kinetically limited by trigger reactions, such as proton shifts.

7. Concluding remarks

Since flash-induced FTIR difference spectra throughout the S-state cycle were reported [29,30], electron and proton transfer reactions and the concomitant structural changes of proteins and water molecules during water oxidation have been investigated using FTIR and

TRIR spectroscopy, which is advantageous over other spectroscopic methods because the structural changes of essentially any chemical species in the system are detectable as changes in IR absorption. Structural changes in amino acid side chains, polypeptide main chains, and water molecules coupled to the Mn_4CaO_5 cluster have been detected using their specific vibrations [20–28]. The electron flow from WOC to the electron acceptor side was monitored using the ferricyanide/ferrocyanide signal, providing information regarding the miss probabilities of individual S-state transitions [77], while the release of protons from substrate water was detected using the IR signal of Mes buffer to estimate the proton release pattern (1, 0, 1 and 2 for $S_0 \rightarrow S_1$, $S_1 \rightarrow S_2$, $S_2 \rightarrow S_3$ and $S_3 \rightarrow S_0$, respectively) [89]. Furthermore, the dynamics of the PCET reactions were investigated using dispersive-type TRIR spectroscopy [31]. In particular, evidence for significant proton movements during the so-called lag phase for ~200 μs [80,81] before electron transfer in the $S_3 \rightarrow S_0$ transition was obtained by the observation of a drastic change at the wavenumber, which represented polarizable protons in hydrogen bond networks [31]. The proton release before electron transfer in the S_3 state was rationalized by the storage of an excess positive charge on the Mn_4CaO_5 cluster in the S_2 and S_3 states, which was revealed by the proton release pattern described above and the abstraction of a single electron at each transition. The higher miss probability in the $S_3 \rightarrow S_0$ transition detected in FTIR [77] was consistent with the presence of the lag phase and slow electron transfer kinetics (1–2 ms) [31,80,81]. In the $S_2 \rightarrow S_3$ transition, a fast proton movement was detected [31], although additional TRIR studies are needed before definitive conclusion can be reached. FTIR analyses also provided information regarding proton transfer pathways and the gating mechanism [68,70,107,108,112,113].

These examples of the applications of IR spectroscopy to the WOC reaction revealed that the FTIR difference and TRIR spectroscopy techniques necessary to investigate the water oxidation mechanism have mostly been established. To obtain further detailed information, such as the roles of specific amino acid residues and water molecules, accurate assignments of the bands in the FTIR spectra of the S-state cycle to individual residues and water molecules surrounding the Mn_4CaO_5 cluster will be necessary. To this end, vibrational analyses of WOC using quantum chemical calculations by the DFT and QM/MM methods are promising. In combination with such theoretical analyses, further IR analyses using site-directed mutagenesis and isotope substitutions are necessary to obtain more specific information. Such information will allow FTIR and TRIR spectroscopy to make a significant contribution to our understanding of the molecular mechanisms underlying photosynthetic water oxidation.

Acknowledgements

I thank Richard Debus for the valuable discussion and sending me a preprint of his work. This study was supported by the Grants-in-Aid for Scientific Research from the Ministry of Education, Culture, Sports, Science, and Technology (24000018, 24107003, and 25291033).

References

[1] R.J. Debus, The manganese and calcium ions of photosynthetic oxygen evolution, Biochim. Biophys. Acta 1102 (1992) 269–352.
[2] W. Hillier, J. Messinger, Mechanism of photosynthetic oxygen production, in: T. Wydrzynski, K. Satoh (Eds.), Photosystem II: The Light-Driven Water:Plastoquinone Oxidoreductase, Springer, Dordrecht, The Netherlands, 2005, pp. 567–608.
[3] J.P. McEvoy, G.W. Brudvig, Water-splitting chemistry of photosystem II, Chem. Rev. 106 (2006) 4455–4483.
[4] J. Messinger, T. Noguchi, J. Yano, Photosynthetic O_2 evolution, in: T. Wydrzynski, W. Hillier (Eds.), Molecular Solar Fuels, Chapter 7, Royal Society of Chemistry, Cambridge, U.K., 2012, pp. 163–207.
[5] G. Renger, Mechanism of light induced water splitting in Photosystem II of oxygen evolving photosynthetic organisms, Biochim. Biophys. Acta 1817 (2012) 1164–1176.
[6] A. Grundmeier, H. Dau, Structural models of the manganese complex of photosystem II and mechanistic implications, Biochim. Biophys. Acta 1817 (2012) 88–105.
[7] D.J. Vinyard, G.M. Ananyev, G.C. Dismukes, Photosystem II: the reaction center of oxygenic photosynthesis, Annu. Rev. Biochem. 82 (2013) 577–606.
[8] N. Cox, J. Messinger, Reflections on substrate water and dioxygen formation, Biochim. Biophys. Acta 1827 (2013) 1020–1030.
[9] B.A. Diner, F. Rappaport, Structure, dynamics, and energetics of the primary photochemistry of photosystem II of oxygenic photosynthesis, Annu. Rev. Plant Biol. 53 (2002) 551–580.
[10] G. Renger, A.R. Holzwarth, Primary electron transfer, in: T. Wydrzynski, K. Satoh (Eds.), Photosystem II: The Light-Driven Water:Plastoquinone Oxidoreductase, Springer, Dordrecht, The Netherlands, 2005, pp. 139–175.
[11] V. Petrouleas, A.R. Crofts, The iron-quinone acceptor complex, in: T. Wydrzynski, K. Satoh (Eds.), Photosystem II: The Light-Driven Water:Plastoquinone Oxidoreductase, Springer, Dordrecht, The Netherlands, 2005, pp. 177–206.
[12] K.N. Ferreira, T.M. Iverson, K. Maghlaoui, J. Barber, S. Iwata, Architecture of the photosynthetic oxygen-evolving center, Science 303 (2004) 1831–1838.
[13] A. Guskov, J. Kern, A. Gabdulkhakov, M. Broser, A. Zouni, W. Saenger, Cyanobacterial photosystem II at 2.9-Å resolution and the role of quinones, lipids, channels and chloride, Nature Struct Mol. Biol. 16 (2009) 334–342.
[14] Y. Umena, K. Kawakami, J.R. Shen, N. Kamiya, Crystal structure of oxygen-evolving photosystem II at a resolution of 1.9 Å, Nature 473 (2011) 55–60.
[15] P.E.M. Siegbahn, Water oxidation mechanism in photosystem II, including oxidations, proton release pathways, O–O bond formation and O_2 release, Biochim. Biophys. Acta 1827 (2013) 1003–1019.
[16] L. Rapatskiy, N. Cox, A. Savitsky, W.M. Ames, J. Sander, M.M. Nowaczyk, M. Rögner, A. Boussac, F. Neese, J. Messinger, W. Lubitz, Detection of the water-binding sites of the oxygen-evolving complex of photosystem II using W-band ^{17}O electron–electron double resonance-detected NMR spectroscopy, J. Am. Chem. Soc. 134 (2012) 16619–16634.
[17] W. Mäntele, Reaction-induced infrared difference spectroscopy for the study of protein function and reaction-mechanisms, Trends Biochem. Sci. 18 (1993) 197–202.
[18] R. Vogel, F. Siebert, Vibrational spectroscopy as a tool for probing protein function, Curr. Opin. Chem. Biol. 4 (2000) 518–523.
[19] C. Berthomieu, R. Hienerwadel, Fourier transform infrared (FTIR) spectroscopy, Photosynth. Res. 101 (2009) 157–170.
[20] H.-A. Chu, W. Hillier, N.A. Law, G.T. Babcock, Vibrational spectroscopy of the oxygen-evolving complex and of manganese model compounds, Biochim. Biophys. Acta 1503 (2001) 69–82.
[21] T. Noguchi, C. Berthomieu, Molecular analysis by vibrational spectroscopy, in: T. Wydrzynski, K. Satoh (Eds.), Photosystem II: The Light-Driven Water:Plastoquinone Oxidoreductase, Springer, Dordrecht, The Netherlands, 2005, pp. 367–387.
[22] T. Noguchi, Light-induced FTIR difference spectroscopy as a powerful tool toward understanding the molecular mechanism of photosynthetic oxygen evolution, Photosynth. Res. 91 (2007) 59–69.
[23] R.J. Debus, Protein ligation of the photosynthetic oxygen-evolving center, Coord. Chem. Rev. 252 (2008) 244–258.
[24] T. Noguchi, Fourier transform infrared analysis of the photosynthetic oxygen-evolving center, Coord. Chem. Rev. 252 (2008) 336–346.
[25] T. Noguchi, FTIR detection of water reactions in the oxygen-evolving center of photosystem II, Phil. Trans. R. Soc. B 363 (2008) 1189–1195.
[26] T. Noguchi, Monitoring the reactions of photosynthetic water oxidation using infrared spectroscopy, Biomed. Spectrosc. Imaging 2 (2013) 115–128.
[27] H.-A. Chu, Fourier transform infrared difference spectroscopy for studying the molecular mechanism of photosynthetic water oxidation, Front. Plant Sci. 4 (2013) 146.
[28] R.J. Debus, FTIR Studies of metal ligands, networks of hydrogen bonds, and water molecules near the active site Mn_4CaO_5 cluster in photosystem II, Biochim. Biophys. 1847 (2015) 19–34.
[29] T. Noguchi, M. Sugiura, Flash-induced Fourier transform infrared detection of the structural changes during the S-state cycle of the oxygen-evolving complex in photosystem II, Biochemistry 40 (2001) 1497–1502.
[30] W. Hillier, G.T. Babcock, S-state dependent Fourier transform infrared difference spectra for the photosystem II oxygen evolving complex, Biochemistry 40 (2001) 1503–1509.
[31] T. Noguchi, H. Suzuki, M. Tsuno, M. Sugiura, C. Kato, Time-resolved infrared detection of the proton and protein dynamics during photosynthetic oxygen evolution, Biochemistry 51 (2012) 3205–3214.
[32] T. Noguchi, M. Sugiura, Flash-induced FTIR difference spectra of the water oxidizing complex in moderately hydrated photosystem II core films: effect of hydration extent on S-state transitions, Biochemistry 41 (2002) 2322–2330.
[33] T. Noguchi, M. Sugiura, FTIR detection of water reactions during the flash-induced S-state cycle of the photosynthetic water oxidizing complex, Biochemistry 41 (2002) 15706–15712.
[34] T. Noguchi, M. Sugiura, Analysis of flash-induced FTIR difference spectra of the S-state cycle in the photosynthetic water-oxidizing complex by uniform ^{15}N and ^{13}C isotope labelling, Biochemistry 42 (2003) 6035–6042.
[35] Y. Kimura, N. Mizusawa, A. Ishii, T. Yamanari, T. Ono, Changes of low-frequency vibrational modes induced by universal ^{15}N- and ^{13}C-isotope labeling in S_2/S_1 FTIR difference spectrum of oxygen-evolving complex, Biochemistry 42 (2003) 13170–13177.
[36] M. Tomita, K. Ifuku, F. Sato, T. Noguchi, FTIR evidence that the PsbP extrinsic protein induces protein conformational changes around the oxygen-evolving Mn cluster in photosystem II, Biochemistry 48 (2009) 6318–6325.
[37] K. Ido, S. Kakiuchi, C. Uno, T. Nishimura, Y. Fukao, T. Noguchi, F. Sato, K. Ifuku, Structure around conserved His144 and Asp165 in the PsbP protein is important for the interaction between its N-terminus and the Cyt b559 subunit of photosystem II, J. Biol. Chem. 287 (2012) 26377–26387.

[38] S. Kakiuchi, C. Uno, K. Ido, T. Nishimura, T. Noguchi, K. Ifuku, F. Sato, The PsbQ protein stabilizes the functional binding of the PsbP protein to photosystem II in higher plants, Biochim. Biophys. Acta 1817 (2012) 1346–1351.

[39] C. Uno, R. Nagao, H. Suzuki, T. Tomo, T. Noguchi, Structural coupling of extrinsic proteins with the oxygen evolving center in red algal photosystem II as revealed by light-induced FTIR difference spectroscopy, Biochemistry 52 (2013) 5705–5707.

[40] T. Nishimura, C. Uno, K. Ido, R. Nagao, T. Noguchi, F. Sato, K. Ifuku, Identification of the basic amino acid residues on the PsbP protein involved in the electrostatic interaction with photosystem II, Biochim. Biophys. Acta 1837 (2014) 1447–1453.

[41] T. Noguchi, T. Ono, Y. Inoue, Direct detection of a carboxylate bridge between Mn and Ca^{2+} in the photosynthetic oxygen-evolving center by means of Fourier transform infrared spectroscopy, Biochim. Biophys. Acta 1228 (1995) 189–200.

[42] H.-A. Chu, W. Hillier, R.J. Debus, Evidence that the C-terminus of the D1 polypeptide of photosystem II is ligated to the manganese ion that undergoes oxidation during the S_1 to S_2 transition: an isotope-edited FTIR study, Biochemistry 43 (2004) 3152–3166.

[43] M.A. Strickler, L.M. Walker, W. Hillier, R.J. Debus, Evidence from biosynthetically incorporated strontium and FTIR difference spectroscopy that the C-terminus of the D1 polypeptide of photosystem II does not ligate calcium, Biochemistry 44 (2005) 8571–8577.

[44] N. Mizusawa, T. Yamanari, Y. Kimura, A. Ishii, S. Nakazawa, T. Ono, Changes in the functional and structural properties of the Mn cluster induced by replacing the side group of the C-terminus of the D1 protein of photosystem II, Biochemistry 43 (2004) 14644–14652.

[45] Y. Kimura, N. Mizusawa, T. Yamanari, A. Ishii, T. Ono, Structural changes of D1 C-terminal α-carboxylate during S-state cycling in photosynthetic oxygen evolution, J. Biol. Chem. 280 (2005) 2078–2083.

[46] M.A. Strickler, H.J. Hwang, R.L. Burnap, J. Yano, L.M. Walker, R.J. Service, R.D. Britt, W. Hillier, R.J. Debus, Glutamate-354 of the CP43 polypeptide interacts with the oxygen evolving Mn_4Ca cluster of photosystem II: a preliminary characterization of the Glu354Gln mutant, Phil. Trans. R. Soc. B 363 (2008) 1179–1188.

[47] Y. Shimada, H. Suzuki, T. Tsuchiya, T. Tomo, T. Noguchi, M. Mimuro, Effect of a single amino acid substitution of the 43 kDa chlorophyll-protein on the oxygen-evolving reaction of the cyanobacterium *Synechocystis* sp. PCC 6803: analysis of the Glu354Gln mutation, Biochemistry 48 (2009) 6095–6103.

[48] R.J. Service, J. Yano, I. McConnell, H.J. Hwang, D. Niks, R. Hille, T. Wydrzynski, R.L. Burnap, W. Hillier, R.J. Debus, Participation of glutamate-354 of the CP43 polypeptide in the ligation of manganese and the binding of substrate water in photosystem II, Biochemistry 50 (2011) 63–81.

[49] R.J. Service, J. Yano, P.L. Dilbeck, R.L. Burnap, W. Hillier, R.J. Debus, Participation of glutamate-333 of the D1 polypeptide in the ligation of the Mn_4CaO_5 cluster in photosystem II, Biochemistry 52 (2013) 8452–8464.

[50] H.-A. Chu, R.J. Debus, G.T. Babcock, D1-Asp170 is structurally coupled to the oxygen evolving complex in photosystem II as revealed by light-induced Fourier transform infrared difference spectroscopy, Biochemistry 40 (2001) 2312–2316.

[51] R.J. Debus, M.A. Strickler, L.M. Walker, W. Hillier, No evidence from FTIR difference spectroscopy that aspartate-170 of the D1 polypeptide ligates a manganese ion that undergoes oxidation during the S_0 to S_1, S_1 to S_2, or S_2 to S_3 transitions in photosystem II, Biochemistry 44 (2005) 1367–1374.

[52] Y. Kimura, N. Mizusawa, A. Ishii, S. Nakazawa, T. Ono, Changes in structural and functional properties of oxygen-evolving complex induced by replacement of D1-glutamate 189 with glutamine in photosystem II — ligation of glutamate 189 carboxylate to the manganese cluster, J. Biol. Chem. 280 (2005) 37895–37900.

[53] M.A. Strickler, W. Hillier, R.J. Debus, No evidence from FTIR difference spectroscopy that glutamate-189 of the D1 polypeptide ligates a Mn ion that undergoes oxidation during the S_0 to S_1, S_1 to S_2, or S_2 to S_3 transitions in photosystem II, Biochemistry 45 (2006) 8801–8811.

[54] M.A. Strickler, L.M. Walker, W. Hillier, R.D. Britt, R.J. Debus, No evidence from FTIR difference spectroscopy that aspartate-342 of the D1 polypeptide ligates a Mn ion that undergoes oxidation during the S_0 to S_1, S_1 to S_2, or S_2 to S_3 transitions in photosystem II, Biochemistry 46 (2007) 3151–3160.

[55] Y. Taguchi, T. Noguchi, Drastic changes in the ligand structure of the oxygen-evolving Mn cluster upon Ca^{2+} depletion as revealed by FTIR difference spectroscopy, Biochim. Biophys. Acta 1767 (2007) 535–540.

[56] H. Suzuki, Y. Taguchi, M. Sugiura, A. Boussac, T. Noguchi, Structural perturbation of the carboxylate ligands to the manganese cluster upon Ca^{2+}/Sr^{2+} exchange in the S-state cycle of photosynthetic oxygen evolution as studied by flash-induced FTIR difference spectroscopy, Biochemistry 45 (2006) 13454–13464.

[57] Y. Kimura, K. Hasegawa, T. Ono, Characteristic changes of the S_2/S_1 difference FTIR spectrum induced by Ca^{2+} depletion and metal cation substitution in the photosynthetic oxygen-evolving complex, Biochemistry 41 (2002) 5844–5853.

[58] H.-A. Chu, Y.-W. Feng, C.-M. Wang, K.-A. Chiang, S.-C. Ke, Ammonia-induced structural changes of the oxygen-evolving complex in photosystem II as revealed by light-induced FTIR difference spectroscopy, Biochemistry 43 (2004) 10877–10885.

[59] C.-H. Fang, K.-A. Chiang, C.-H. Hung, K. Chang, S.-C. Ke, H.-A. Chu, Effects of ethylene glycol and methanol on ammonia-induced structural changes of the oxygen-evolving complex in photosystem II, Biochemistry 44 (2005) 9758–9765.

[60] L.-H. Hou, C.-M. Wu, H.-H. Huang, H.-A. Chu, Effects of ammonia on the structure of the oxygen-evolving complex in photosystem II as revealed by light-induced FTIR difference spectroscopy, Biochemistry 50 (2011) 9248–9254.

[61] M. Tsuno, H. Suzuki, T. Kondo, H. Mino, T. Noguchi, Interaction and inhibitory effect of ammonium cation in the oxygen evolving center of photosystem II, Biochemistry 50 (2011) 2506–2514.

[62] K. Hasegawa, Y. Kimura, T. Ono, Chloride cofactor in the photosynthetic oxygen-evolving complex studied by Fourier transform infrared spectroscopy, Biochemistry 41 (2002) 13839–13850.

[63] K. Hasegawa, Y. Kimura, T. Ono, Oxidation of the Mn cluster induces structural changes of NO_3^- functionally bound to the Cl^- site in the oxygen-evolving complex of photosystem II, Biophys. J. 86 (2004) 1042–1050.

[64] T. Noguchi, Y. Inoue, X.-S. Tang, Structure of a histidine ligand in the photosynthetic oxygen-evolving complex as studied by light-induced Fourier transform infrared difference spectroscopy, Biochemistry 38 (1999) 10187–10195.

[65] Y. Kimura, N. Mizusawa, A. Ishii, T. Ono, FTIR detection of structural changes in a histidine ligand during S-state cycling of photosynthetic oxygen-evolving complex, Biochemistry 44 (2005) 16072–16078.

[66] Y. Shimada, H. Suzuki, T. Tsuchiya, M. Mimuro, T. Noguchi, Structural coupling of an arginine side chain with the oxygen evolving Mn_4Ca cluster in photosynstem II as revealed by isotope-edited Fourier transform infrared spectroscopy, J. Am. Chem. Soc. 133 (2011) 3808–3811.

[67] T. Noguchi, M. Sugiura, Structure of an active water molecule in the water oxidizing complex of photosystem II as studied by FTIR spectroscopy, Biochemistry 39 (2000) 10943–10949.

[68] R.J. Debus, Evidence from FTIR difference spectroscopy that D1-Asp61 influences the water reactions of the oxygen-evolving Mn_4CaO_5 cluster of photosystem II, Biochemistry 53 (2014) 2941–2955.

[69] B.C. Polander, B.A. Barry, Detection of an intermediary, protonated water cluster in photosynthetic oxygen evolution, Proc. Natl. Acad. Sci. U. S. A. 110 (2013) 10634–10639.

[70] S. Nakamura, R. Nagao, R. Takahashi, T. Noguchi, FTIR detection of a polarizable proton trapped between photooxidized tyrosine Yz and a coupled histidine in photosystem II: relevance to the proton transfer mechanism of water oxidation, Biochemistry 53 (2014) 3131–3144.

[71] E.M. Sproviero, J.A. Gascon, J.P. McEvoy, G.W. Brudvig, V.S. Batista, Quantum mechanics/molecular mechanics study of the catalytic cycle of water splitting in photosystem II, J. Am. Chem. Soc. 130 (2008) 3428–3442.

[72] H. Suzuki, M. Sugiura, T. Noguchi, Monitoring water reactions during the S-state cycle of the photosynthetic water-oxidizing center: detection of the DOD bending vibrations by means of Fourier transform infrared spectroscopy, Biochemistry 47 (2008) 11024–11030.

[73] R. de Wijn, H.J. van Gorkom, The rate of charge recombination in Photosystem II, Biochim. Biophys. Acta 1553 (2002) 302–308.

[74] J. Messinger, G. Renger, Photosynthetic water-splitting, in: G. Renger (Ed.), Primary Processes of Photosynthesis, Part 2: Principles and Apparatus, The Royal Society of Chemistry, Cambridge, UK, 2008, pp. 291–349.

[75] S. Isgandarova, G. Renger, J. Messinger, Functional differences of photosystem II from *Synechococcus elongatus* and spinach characterized by flash induced oxygen evolution patterns, Biochemistry 42 (2003) 8929–8938.

[76] J. Lavergne, Improved UV-visible spectra of the S-transitions in the photosynthetic oxygen-evolving system, Biochim. Biophys. Acta 1060 (1991) 175–188.

[77] H. Suzuki, M. Sugiura, T. Noguchi, Determination of the miss probabilities of individual S-state transitions during photosynthetic water oxidation by monitoring electron flow in photosystem II using FTIR spectroscopy, Biochemistry 51 (2012) 6776–6785.

[78] R. de Wijn, H.J. van Gorkom, S-state dependence of the miss probability in Photosystem II, Photosynth. Res. 72 (2002) 217–222.

[79] R. de Wijn, T. Schrama, H.J. van Gorkom, Secondary stabilization reactions and proton-coupled electron transport in photosystem II investigated by electroluminescence and fluorescence spectroscopy, Biochemistry 40 (2001) 5821–5834.

[80] F. Rappaport, M. Blanchard-Desce, J. Lavergne, Kinetics of electron-transfer and electrochromic change during the redox transitions of the photosynthetic oxygen-evolving complex, Biochim. Biophys. Acta 1184 (1994) 178–192.

[81] M. Haumann, P. Liebisch, C. Müller, M. Barra, M. Grabolle, H. Dau, Photosynthetic O_2 formation tracked by time-resolved X-ray experiments, Science 310 (2005) 1019–1021.

[82] G. Han, F. Mamedov, S. Styring, Misses during water oxidation in photosystem II are S state-dependent, J. Biol. Chem. 287 (2012) 13422–13429.

[83] V. Förster, W. Junge, Stoichiometry and kinetics of proton release upon photosynthetic water oxidation, Photochem. Photobiol. 41 (1985) 183–190.

[84] J. Lavergne, W. Junge, Proton release during the redox cycle of the water oxidase, Photosynth. Res. 38 (1993) 279–296.

[85] M. Haumann, W. Junge, Protons and charge indicators in oxygen evolution, in: D.R. Ort, C.F. Yocum (Eds.), Oxygenic Photosynthesis: The Light Reactions, vol. 4, Kluwer Academic Publishers, Dordrecht, The Netherlands, 1996, pp. 165–192.

[86] W. Junge, M. Haumann, R. Ahlbrink, A. Mulkidjanian, J. Clausen, Electrostatics and proton transfer in photosynthetic water oxidation, Phil. Trans. R. Soc. B 357 (2002) 1407–1417.

[87] F. Rappaport, J. Lavergne, Coupling of electron and proton transfer in the photosynthetic water oxidase, Biochim. Biophys. Acta 1503 (2001) 246–259.

[88] E. Schlodder, H.T. Witt, Stoichiometry of proton release from the catalytic center in photosynthetic water oxidation — reexamination by a glass electrode study at pH 5.5–7.2, J. Biol. Chem. 274 (1999) 30387–30392.

[89] H. Suzuki, M. Sugiura, T. Noguchi, Monitoring proton release during photosynthetic water oxidation in photosystem II by means of isotope-edited infrared spectroscopy, J. Am. Chem. Soc. 131 (2009) 7849–7857.

[90] H. Suzuki, M. Sugiura, T. Noguchi, pH dependence of the flash-induced S-state transitions in the oxygen-evolving center of photosystem II from *Thermosynechoccocus elongatus* as revealed by Fourier transform infrared spectroscopy, Biochemistry 44 (2005) 1708–1718.

[91] G. Bernát, F. Morvaridi, Y. Feyziyev, S. Styring, pH dependence of the four individual transitions in the catalytic S-cycle during photosynthetic oxygen evolution, Biochemistry 41 (2002) 5830–5843.
[92] A. Klauss, M. Haumann, H. Dau, Alternating electron and proton transfer steps in photosynthetic water oxidation, Proc. Natl. Acad. Sci. U. S. A. 109 (2012) 16035–16040.
[93] J. Wang, M.A. El-Sayed, Time-resolved Fourier transform infrared spectroscopy of the polarizable proton continua and the proton pump mechanism of bacteriorhodopsin, Biophys. J. 80 (2001) 961–971.
[94] F. Garczarek, K. Gerwert, Functional waters in intraprotein proton transfer monitored by FTIR difference spectroscopy, Nature 439 (2006) 109–112.
[95] E. Freier, S. Wolf, K. Gerwert, Proton transfer via a transient linear water-molecule chain in a membrane protein, Proc. Natl. Acad. Sci. U. S. A. 108 (2011) 11435–11439.
[96] G. Christen, F. Reifarth, G. Renger, On the origin of the '35-μs kinetics' of $P680^{+}$• reduction in photosystem II with an intact water oxidising complex, FEBS Lett. 429 (1998) 49–52.
[97] F.M. Ho, S. Styring, Access channels and methanol binding site to the $CaMn_4$ cluster in Photosystem II based on solvent accessibility simulations, with implications for substrate water access, Biochim. Biophys. Acta 1777 (2008) 140–153.
[98] S. Vassiliev, T. Zaraiskaya, D. Bruce, Exploring the energetics of water permeation in photosystem II by multiple steered molecular dynamics simulations, Biochim. Biophys. Acta 1817 (2012) 1671–1678.
[99] K. Ogata, T. Yuki, M. Hatakeyama, W. Uchida, S. Nakamura, All-atom molecular dynamics simulation of photosystem II embedded in thylakoid membrane, J. Am. Chem. Soc. 135 (2013) 15670–15673.
[100] H. Ishikita, W. Saenger, B. Loll, J. Biesiadka, E.W. Knapp, Energetics of a possible proton exit pathway for water oxidation in photosystem II, Biochemistry 45 (2006) 2063–2071.
[101] A. Gabdulkhakov, A. Guskov, M. Broser, J. Kern, F. Muh, W. Saenger, A. Zouni, Probing the accessibility of the Mn_4Ca cluster in photosystem II: channels calculation, noble gas derivatization, and cocrystallization with DMSO, Structure 17 (2009) 1223–1234.
[102] J.W. Murray, J. Barber, Structural characteristics of channels and pathways in photosystem II including the identification of an oxygen channel, J. Struct. Biol. 159 (2007) 228–237.
[103] P.E.M. Siegbahn, Mechanisms for proton release during water oxidation in the S_2 to S_3 and S_3 to S_4 transitions in photosystem II, Phys. Chem. Chem. Phys. 14 (2012) 4849–4856.
[104] K. Linke, F.M. Ho, Water in Photosystem II: structural, functional and mechanistic considerations, Biochim. Biophys. Acta 1837 (2014) 14–32.
[105] H. Bao, P.L. Dilbeck, R.L. Burnap, Proton transport facilitating water-oxidation: the role of second sphere ligands surrounding the catalytic metal cluster, Photosynth. Res. 116 (2013) 215–229.
[106] R. Pokhrel, I.L. McConnell, G.W. Brudvig, Chloride regulation of enzyme turnover: application to the role of chloride in photosystem II, Biochemistry 50 (2011) 2725–2734.
[107] H. Suzuki, J. Yu, T. Kobayashi, H. Nakanishi, P. Nixon, T. Noguchi, Functional roles of D2-Lys317 and the interacting chloride ion in the water oxidation reaction of photosystem II as revealed by Fourier transform infrared analysis, Biochemistry 52 (2013) 4748–4757.
[108] R. Pokhrel, R.J. Service, R.J. Debus, G.W. Brudvig, Mutation of lysine 317 in the D2 subunit of photosystem II alters chloride binding and proton transport, Biochemistry 52 (2013) 4758–4773.
[109] J. Clausen, R.J. Debus, W. Junge, Time-resolved oxygen production by PSII: chasing chemical intermediates, Biochim. Biophys. Acta 1655 (2004) 184–194.
[110] M. Hundelt, A.M. Hays, R.J. Debus, W. Junge, Oxygenic photosystem II: the mutation D1-D61N in *Synechocystis* sp. PCC 6803 retards S-state transitions without affecting electron transfer from Y_Z to $P680^{+}$, Biochemistry 37 (1998) 14450–14456.
[111] P.L. Dilbeck, H.J. Hwang, I. Zaharieva, L. Gerencser, H. Dau, R.L. Burnap, The D1-D61N mutation in *Synechocystis* sp. PCC 6803 allows the observation of pH-sensitive intermediates in the formation and release of O_2 from photosystem II, Biochemistry 51 (2012) 1079–1091.
[112] R.J. Service, W. Hillier, R.J. Debus, Evidence from FTIR difference spectroscopy of an extensive network of hydrogen bonds near the oxygen-evolving Mn_4Ca cluster of photosystem II involving D1-Glu65, D2-Glu312, and D1-Glu329, Biochemistry 49 (2010) 6655–6669.
[113] R.J. Service, W. Hillier, R.J. Debus, Network of hydrogen bonds near the oxygen-evolving Mn_4CaO_5 cluster of photosystem II probed with FTIR difference spectroscopy, Biochemistry 53 (2014) 1001–1017.
[114] J. Sinclair, The influence of anions on oxygen evolution by isolated spinach chloroplasts, Biochim. Biophys. Acta 764 (1984) 247–252.
[115] H. Wincencjusz, C.F. Yocum, H.J. van Gorkom, Activating anions that replace Cl^{-} in the O_2-evolving complex of photosystem II slow the kinetics of the terminal step in water oxidation and destabilize the S_2 and S_3 states, Biochemistry 38 (1999) 3719–3725.
[116] A. Boussac, N. Ishida, M. Sugiura, F. Rappaport, Probing the role of chloride in Photosystem II from *Thermosynechococcus elongatus* by exchanging chloride for iodide, Biochim. Biophys. Acta 1817 (2012) 802–810.
[117] H. Wincencjusz, H.J. van Gorkom, C.F. Yocum, The photosynthetic oxygen evolving complex requires chloride for its redox state $S_2 \rightarrow S_3$ and $S_3 \rightarrow S_0$ transitions but not for $S_0 \rightarrow S_1$ or $S_1 \rightarrow S_2$ transitions, Biochemistry 36 (1997) 3663–3670.
[118] B. Diner, R.D. Britt, The redox-active tyrosine Y_Z and Y_D, in: T. Wydrzynski, K. Satoh (Eds.), Photosystem II: The Light-Driven Water:Plastoquinone Oxidoreductase, Springer, Dordrecht, The Netherlands, 2005, pp. 207–233.
[119] S. Styring, J. Sjöholm, F. Mamedov, Two tyrosines that changed the world: interfacing the oxidizing power of photochemistry to water splitting in photosystem II, Biochim. Biophys. Acta 1817 (2012) 76–87.
[120] A.M.A. Hays, I.R. Vassiliev, J.H. Golbeck, R.J. Debus, Role of D1-His190 in the proton-coupled oxidation of tyrosine Y_Z in manganese-depleted photosystem II, Biochemistry 38 (1999) 11851–11865.
[121] F. Rappaport, A. Boussac, D.A. Force, J. Peloquin, M. Brynda, M. Sugiura, S. Un, R.D. Britt, B.A. Diner, Probing the coupling between proton and electron transfer in photosystem II core complexes containing a 3-fluorotyrosine, J. Am. Chem. Soc. 131 (2009) 4425–4433.
[122] K. Saito, J.R. Shen, T. Ishida, H. Ishikita, Short hydrogen bond between redox-active tyrosine Y_Z and D1-His190 in the photosystem II crystal structure, Biochemistry 50 (2011) 9836–9844.
[123] C. Berthomieu, R. Hienerwadel, A. Boussac, J. Breton, B.A. Diner, Hydrogen bonding of redox-active tyrosine Z of photosystem II probed by FTIR difference spectroscopy, Biochemistry 37 (1998) 10547–10554.
[124] P.J. O'Malley, Density functional studies of phenoxyl-Na^{+} ion complexes: implications for tyrosyl free radical interactions in vitro, Chem. Phys. Lett. 325 (2000) 69–72.
[125] P.J. O'Malley, Density functional calculations modelling tyrosine oxidation in oxygenic photosynthetic electron transfer, Biochim. Biophys. Acta 1553 (2002) 212–217.
[126] C.J.T. de Grotthuss, Sur la décomposition de l'eau et des corps qu'elle tient en dissolution à l'aide de l'électricité galvanique, Ann. Chim. 58 (1806) 54–73.
[127] C.W. Hoganson, G.T. Babcock, A metalloradical mechanism for the generation of oxygen from water in photosynthesis, Science 277 (1997) 1953–1956.
[128] K. Kawakami, Y. Umena, N. Kamiya, J.R. Shen, Structure of the catalytic, inorganic core of oxygen-evolving photosystem II at 1.9 Å resolution, J. Photochem. Photobiol. B 104 (2011) 9–18.